Sun *et al. Cancer Cell International* (2024) 24:350
https://doi.org/10.1186/s12935-024-03543-7

Cancer Cell International

RESEARCH Open Access

Identification and validation of a prognostic model based on three TLS-Related genes in oral squamous cell carcinoma

Bincan Sun[1,8], Chengwen Gan[5], Yan Tang[6], Qian Xu[1,2,3], Kai Wang[7] and Feiya Zhu[1,2,3,4*]

Abstract

Background The tertiary lymphoid structures (TLSs) have an immunomodulatory function and have a positive impact on the survival outcomes of patients with oral squamous cell carcinoma (OSCC). However, there is a lack of standard approaches for quantifying TLSs and prognostic models using TLS-related genes (TLSRGs). These limitations limit the widespread use of TLSs in clinical practice.

Methods A convolutional neural network was used to automatically detect and quantify TLSs in HE-stained whole slide images. By employing bioinformatics and diverse statistical methods, this research created a prognostic model using TCGA cohorts and explored the connection between this model and immune infiltration. The expression levels of three TLSRGs in clinical specimens were detected by immunohistochemistry. To facilitate the assessment of individual prognostic outcomes, we further constructed a nomogram based on the risk score and other clinical factors.

Results TLSs were found to be an independent predictor of both overall survival (OS) and disease-free survival in OSCC patients. A larger proportion of the TLS area represented a better prognosis. After analysis, we identified 69 differentially expressed TLSRGs and selected three pivotal TLSRGs to construct the risk score model. This model emerged as a standalone predictor for OS and exhibited close associations with CD4 + T cells, CD8 + T cells, and macrophages. Immunohistochemistry revealed high expression levels of CCR7 and CXCR5 in TLS + OSCC samples, while CD86 was highly expressed in TLS- OSCC samples. The nomogram demonstrates excellent predictive ability for overall survival in OSCC patients.

Conclusions This is the first prognostic nomogram based on TLSRGs, that can effectively predict survival outcomes and contribute to individual treatment strategies for OSCC patients.

Keywords Oral squamous cell carcinoma, Tertiary lymphoid structure, Prognostic model, Immune infiltration, Convolutional neural network

*Correspondence:
Feiya Zhu
188102160@csu.edu.cn

Full list of author information is available at the end of the article

Background

Oral squamous cell carcinoma (OSCC) is the most common type of head and neck squamous cell carcinoma (HNSCC), and is characterized by a notable tendency for metastasis to cervical lymph nodes at a high rate [1, 2]. According to the Global Cancer Observatory (GCO), there were 389,846 diagnosed cases in 2022, including 188,438 deaths. There will be a growth in incidence and mortality until 2040, as predicted by the GCO. Currently, prognosis prediction for patients primarily involves assessing tumor dimensions, lymph nodes and distant organ metastases [3]. However, the prognoses of patients with identical tumor node metastasis (TNM) stages are different, which shows that the TNM stage may fail to capture the immune heterogeneity of OSCC [4, 5].

The tertiary lymphoid structures (TLSs), an ectopic lymphoid organ that forms in nonlymphoid tissues [6], are correlated with favorable clinical outcomes and an improved response to immunological therapy [7–10] across various cancers [11–16]. In the absence of external fibrous capsules, TLSs are directly exposed to the tumor microenvironment and have a stronger specific immune response than other noninfiltrating lymphocytes [7, 17, 18]. A recent study revealed that TLSs serve as an innovative prognostic indicator in the field of HNSCC [19]. The presence of TLSs, which is frequently observed in oral tongue squamous cell carcinoma (OTSCC), is utilized for predicting immunotherapy sensitivity [20]. Furthermore, the presence of TLSs independently correlates with the overall survival (OS) rate and disease-free survival (DFS) rate in patients of OSCC [21]. Thus, TLSs have the potential to be a complementary indicator for predicting clinical outcomes after OSCC surgery. Although TLSs have received increasing attention in prognostic evaluation, there is still no recommended TLS-related molecular marker for building a prognostic model for the accurate stratification of OSCC patients, which limits the ability of TLSs to help clinicians make personalized clinical decisions.

In this study, we used the convolutional neural network (CNN) to automatically identify and quantify TLSs in hematoxylin and eosin (HE) stained whole slide images (WSIs) of OSCC [22], aiming to make the assessment of TLSs more efficient and accurate. We explored TLS-related genes (TLSRGs) related to OSCC through bioinformatics analysis. Based on the TLSRGs, we established a risk score model capable of predicting the prognosis of OSCC patients and evaluated the tumor immune microenvironment. By introducing clinical variables into the model, we constructed a nomogram model [5] aimed at providing individualized evaluations for OSCC patients.

Methods

Data acquisition

High-throughput sequence data and corresponding clinicopathological information for 503 HNSCC (Additional file 1) and 54 adjacent normal mucosa tissues were downloaded from The Cancer Genome Atlas (TCGA) [23]. According to the tumor location, the clinical information and data of 336 OSCC tissues were extracted for subsequent analysis. Patients lacking survival information were omitted from the prognostic analysis. The HE-stained images were downloaded from the Cancer Digital Slide Archive [24].

TLSs quantification

Using the CNN, the presence of TLSs was identified in HE-stained WSIs of OSCC patients. This approach can be used to determine the area occupied by TLSs and their density, and establish a heatmap of lymphocytes [22], which allows us to define TLSs in tissues. Firstly, the modified DeepLab v3 + CNN [25, 26] was used to detect the candidate TLS regions in the original HE-stained images, and the active contour model was applied to optimize the boundaries of the candidate TLS regions. Then, lymphocytes were segmented to identify the following features: number of lymphocytes, size of TLS region, and the density. The candidate regions were considered as TLSs when the number of lymphocytes was greater than 45 and the area was greater than 6245μm^2. TLSs were categorized into three types based on a previously published scale [27, 28]: [1] lymphoid aggregates (Agg), characterized by indistinct masses of lymphocytes; [2] primary follicle-like TLSs (FL1), comprising immature TLSs composed of round lymphocytes lacking germinal centers; and [3] secondary follicle-like TLSs (FL2), representing mature TLSs as round clusters of lymphocytes with the formation of germinal centers. Patients were categorized as TLS + if they had at least one TLS and as TLS- if they had no TLSs. Among TLS + tumors, patients with an area proportion above the series median were categorized into the high-TLS group, while patients with an area proportion below the series median were classified into the low-TLS group. The TLS + tumors could also be classified as follows: [1] Agg + FL1 group: tumors comprising at least one FL1, without FL2, with or without Agg; and [2] Agg + FL1 + FL2 group: tumors containing at least one FL2, irrespective of the presence of Agg and FL1.

DEGs, GO, KEGG analyses

Both TLS + OSCC tissues and TLS- OSCC tissues were compared with normal tissues for differential analysis. Analysis of differentially expressed genes (DEGs) was performed using the R package in combination

with the Wilcoxon test. Visualization of the data was accomplished through the creation of heatmaps using the pheatmap package [29], complemented by the generation of volcano plots using R software. Based on the Gene Ontology (GO) [30] and Kyoto Encyclopedia of Genes and Genomes (KEGG) [31] databases, we performed functional enrichment analysis of TLSRGs using the clusterProfiler package [32]. Those functional categories with an adjusted p-value < 0.05 were regarded as significantly enriched.

Construction of the risk score model and prognostic nomogram

Univariate Cox regression analysis was utilized to assess the relationship between TLSRGs and OS in the TCGA cohort. To prevent overfitting and streamline the gene selection process, stepwise Cox regression analysis was utilized to identify the optimal genes based on genes detected via the Lasso algorithm. The risk score was computed by multiplying gene expression with a linear combination of regression coefficients derived from the Cox regression analysis. Patients were stratified into a high-risk group and a low-risk group based on the median risk score. Kaplan-Meier (K-M) survival curves were generated to compare OS between the low- and high-risk groups. The precision of the risk score model was evaluated through receiver operating characteristic (ROC) curve analysis via the survival ROC package [33]. To explore the role of risk score in evaluating prognosis, we used the Cox regression model to perform a multivariate analysis of risk score and other clinical factors (e.g., gender, age, tumor grade, perineural invasion, nodal extracapsular spread, lymph node neck dissection) to obtain independent factors for OSCC. To facilitate the assessment of individual prognostic risk, we further constructed a nomogram based on the independent factors. The nomogram's predictive precision was evaluated through calibration curves and C-index, ensuring its reliability and effectiveness in forecasting outcomes.

Immune cell infiltration estimation

To investigate the relationship between the presence of TLSs and immune cell infiltration, we used the Tumor Immune Estimation Resource (TIMER) [34], which can estimate the levels of six tumor-infiltrating immune subsets. Relationships between the risk score model and six types of immune cells were analyzed with Pearson's correlation coefficient. The same method was utilized to evaluate the correlations between the proportion of TLS area and six immune cell types.

Tissue samples

Primary OSCC tissues and adjacent normal mucosa tissues, surgically resected at the Department of Oral and Maxillofacial Surgery of the Second Xiangya Hospital between April 2010 and July 2013, were utilized in this study. Participants who received chemotherapy, radiation, or preoperative interventions were ineligible for participation in this study.

Immunohistochemistry

The formalin-fixed paraffin-embedded specimens were sectioned into 4 μm slices for immunohistochemical staining. The sections were baked at 60 °C for 2 h and subsequently dewaxed with xylene. Different concentrations of alcohol were utilized for hydration treatment, and antigen extraction was performed by citrate solution combined with high-pressure repair. Upon cooling, endogenous peroxidase was removed from tissue sections using 3% hydrogen peroxide, followed by triple rinsing with freshly prepared PBS. To mitigate nonspecific binding, the sections were incubated for 60 min in goat serum. The sections were placed in a humidified box at 4 °C, where they were incubated with primary antibodies (anti-CCR7, Proteintech, 25898-1-AP, 1:200; anti-CXCR5, Abcam, ab254415, 1:400; anti-CD86, Abcam, ab269587, 1:100) overnight. Following washing, the sections were treated with secondary antibodies for 60 min at 37 °C. After washing, the sections were stained with DAB and hematoxylin.

Statistical analyses

The data from the experiments were rigorously analyzed with GraphPad Prism 8.0, R software v4.0.1, and ImageJ to ensure precision. For comparisons between two groups, we applied the Student's t test and Wilcoxon test. K-M analysis was used to construct survival curves, and the log-rank test was used to compare survival variances across groups. Univariate and multivariate Cox regression analyses were employed to determine the OS-related prognostic factors. $P < 0.05$ was considered to indicate statistical significance. *, **, and *** represent $p < 0.05$, $p < 0.01$, and $p < 0.001$, respectively.

Results

Clinicopathological characteristics and TLSs expression of OSCC patients

In our analysis of 336 OSCC patients from the TCGA database, we collected data on various clinicopathological characteristics: age (< or ≥60 years), gender, smoking, drinking, pT classification, pN classification, pTNM classification, grade, perineural invasion (PNI), and nodal extracapsular spread (NES). These features are summarized in Table 1. Then the CNN was used

Table 1 Associations between clinicopathological characteristics and TLSs expression in 336 OSCC patients in the TCGA cohort

variable (No.)	Negative (173)	Positive (163)	*p*
Age (Years)			0.442
< 60	71(41%)	74(45.4%)	
≥ 60	102 (59.0%)	89 (54.6%)	
Gender			0.707
Male	131 (75.7%)	120 (73.6%)	
Female	42 (24.3%)	43 (26.4%)	
Smoking			1
Yes	80 (46.2%)	76 (46.6%)	
No	93 (53.8%)	87 (53.4%)	
Drinking			0.639
Yes	117 (67.6%)	108 (66.3%)	
No	56 (32.4%)	55 (33.7%)	
pT classification			**0.003**
T1 ~ T2	51 (29.5%)	74 (45.4%)	
T3 ~ T4	122 (70.5%)	89 (54.6%)	
pN classification			**0.003**
N0	55 (31.7%)	79 (48.5%)	
N1 ~ N3	118 (68.2%)	84 (51.5%)	
pTNM classification			**0.032**
Stage I ~ Stage II	28(16.2%)	42(25.8%)	
Stage III ~ Stage IV	145 (83.8%)	121 (74.2%)	
Grade			0.383
G1 ~ G2	125 (72.2%)	125 (76.7%)	
G3 ~ G4	48 (27.7%)	38 (23.3%)	
Perineural invasion			**0.013**
Positive	83 (47.9%)	58 (35.6%)	
Negative	90 (52.1%)	105 (64.4%)	
Nodal extracapsular spread			**0.022**
Gross Extension	37 (21.4%)	25 (15.3%)	
Microscopic Extension	46 (26.6%)	29 (17.8%)	
No Extranodal Extension	90 (52.0%)	109 (66.9%)	

to determine the three types of TLSs and their respective area proportions in routine HE-stained WSIs, which were obtained from the TCGA database (Fig. 1). We identified 265 TLS + samples among the 336 OSCC samples, and the TLS area accounted for 0.1–6.2% of the total tumor area (mean 2.8%). Among the TLS + OSCC samples, ninety cases (34.0%) were Agg-type TLSs, one hundred cases (37.7%) were FL1-type TLSs, and seventy-five cases (28.3%) were FL2-type TLSs (Additional file 2). Our research investigated the correlations between TLSs expression and clinicopathological parameters in 336 OSCC patients. The results revealed that the occurrence of TLSs was negatively correlated with the pT classification ($p = 0.003$), pN classification ($p = 0.003$), and pTNM classification ($p = 0.032$). In addition to the PNI ($p = 0.013$), TLS + OSCC was also negatively correlated with the NES ($p = 0.022$, Table 1).

TLSs correlated with a positive prognosis in OSCC patients

Then the prognostic significance of TLSs in OSCC patients was assessed. According to the K-M survival analyses, TLS + OSCC was correlated with good OS and DFS (Fig. 2A, D). Based on the TLSs classification in the Methods section, we conducted subgroup analyses of TLS + OSCC patients. Compared with those in the low-TLS group, OS and DFS in the high-TLS group improved significantly (Fig. 2B, E). The K-M survival assessments indicated enhanced OS for patients in the Agg + FL1 + FL2 group compared with those in the Agg + FL1 group. Conversely, disease-free survival (DFS) rates between these groups showed no notable disparity (Fig. 2C, F). These results revealed that the presence of TLSs was a good prognostic indicator for OSCC patients, and patients with a greater proportion of TLSs had better OS and DFS.

To evaluate the potential of TLSs as a standalone predictor of outcomes in OSCC patients, we performed both univariate and multivariate Cox regression analyses. According to the univariate analysis, older age (> 60 years, hazard ratio (HR) = 1.022; 95% confidence interval (CI), 1.009–1.036; $p < 0.001$), pT3-4 stage (HR = 1.868; 95% CI, 1.375–2.539; $p < 0.001$), and lymph node metastasis (HR = 1.523; 95% CI, 1.148–2.021; $p = 0.004$) were linked to an elevated risk of OS, while the gender (male, HR = 0.737; 95% CI, 0.551–0.987; $p = 0.040$) and the presence of TLSs (HR = 0.430; 95% CI, 0.324–0.572; $p < 0.001$) were correlated with a reduced risk (Fig. 2G). According to the multivariate analysis, age, pT stage, lymph node metastasis status, and TLSs were found to be independent prognostic factors for the OS rate of OSCC patients. Specifically, only the presence of TLSs (HR = 0.484; 95% CI, 0.361–0.649; $p < 0.001$) was linked to a decreased risk of mortality (Fig. 2H).

Differential expression of genes in TLS + and TLS- OSCC tissues

TLS + and TLS- OSCC tissues were compared with normal mucosa tissues to identify DEGs. The heatmaps clearly distinguished between OSCC samples and normal samples based on the DEGs (Fig. 3A and D). The volcano plots revealed that 13 DEGs were downregulated and 203 DEGs were upregulated in the TLS + OSCC group (Fig. 3B), while 32 DEGs were downregulated and 207 DEGs were upregulated in the TLS-OSCC group (Fig. 3E). By comparing the upregulated DEGs in the TLS + and TLS − groups, we obtained 64 DEGs via a Venn diagram. Similarly, we obtained 5 DEGs that were downregulated in the TLS + OSCC tissues but not in the TLS- OSCC tissues. These 69 (64 + 5) DEGs, defined as TLSRGs, were used for further modeling (Fig. 3C).

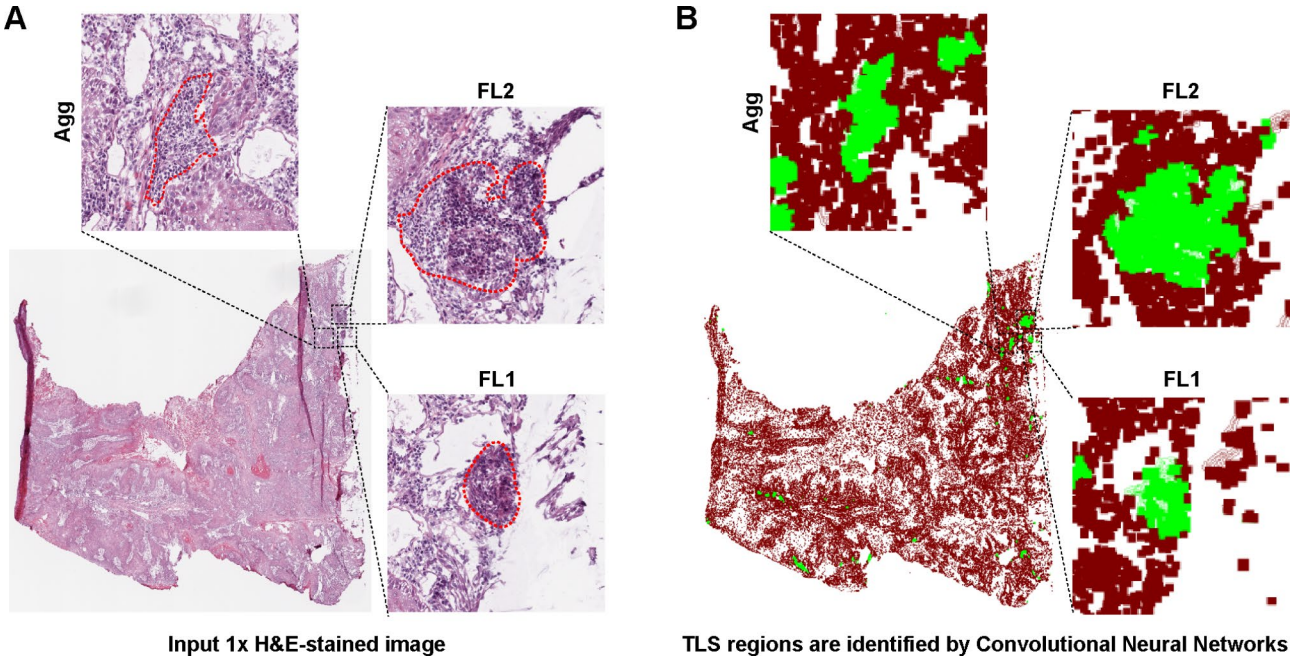

Fig. 1 Identification of TLS regions. (**A**) 1x HE-stained whole slide image of OSCC tissues. Red dashed area, identified TLS regions. (**B**) Heatmap of TLS regions. Green area, identified TLS regions; dark red area, non-TLS organization structure

To further explore the biological functions of the TLSRGs, we conducted GO and KEGG analyses on the 69 TLSRGs. GO analysis identified the primary functional categories in biological processes as the chemokine-mediated signaling pathway, regulation of dendritic cell antigen processing and presentation, and dendritic cell apoptotic process. Regarding molecular function, these TLSRGs were mainly involved in receptor-ligand activity and cytokine activity. KEGG analysis revealed that the TLSRGs were associated with cytokine-cytokine receptor interaction and chemokine signaling pathway (Fig. 3F).

Construction and identification of a prognostic model for OSCC

To determine whether the TLSRGs were associated with patient clinical outcomes, the 69 TLSRGs were evaluated by univariate Cox regression analysis (Additional Table 1). A total of 11 TLSRGs significantly influenced the OS of OSCC patients (Fig. 4A). These 11 TLS-related genes (TLSRGs) were subjected to Lasso Cox analysis, resulting in the filtration of 9 genes. (Fig. 4B). Stepwise Cox regression analysis was subsequently performed, and three key TLSRGs (CD86, CXCR5, and CCR7) were chosen to construct a model for prediction (Table 2). The model formula was as follows: risk score = (0.3169 × CD86 expression) + (-1.3345× CXCR5 expression) + (-0.2974 × CCR7 expression). TLSs signatures reported in HNSCC and other cancer studies were summarized in Additional Table 2, and our key genes CXCR5 and CCR7 were also in the TLSs gene signature list for HNSCC. With respect to the median risk score, the OSCC patients were then divided into two groups: one at high risk and the other at low risk (Fig. 4C). The patients' survival time and the heatmaps of the three TLSRGs are presented in Fig. 4D and E. These findings indicated a direct correlation between heightened risk scores and elevated CD86 expression, concurrently revealing a decrease in CXCR5 and CCR7 expression. An increased risk score was also accompanied by a decrease in survival time. The K-M curve demonstrated that the survival rate of the low-risk group ($n=165$) was markedly greater than that of the high-risk group ($n=165$) (Fig. 4F). Additionally, the ROC curves revealed AUC values of 0.674, 0.652, and 0.549 for 1, 3, and 5 years respectively, suggesting that the prognostic model exhibited good sensitivity and specificity (Fig. 4G).

Correlations between the prognostic model and clinical parameters

To further substantiate the reliability of the model, we investigated the correlations between the expression levels of the three key TLSRGs and clinical data in OSCC patients. First, our research focused on the correlations between survival outcomes and the expression of the three TLSRGs in OSCC patients. The K-M survival analyses revealed that the elevated expressions of CCR7 and CXCR5 were directly correlated with

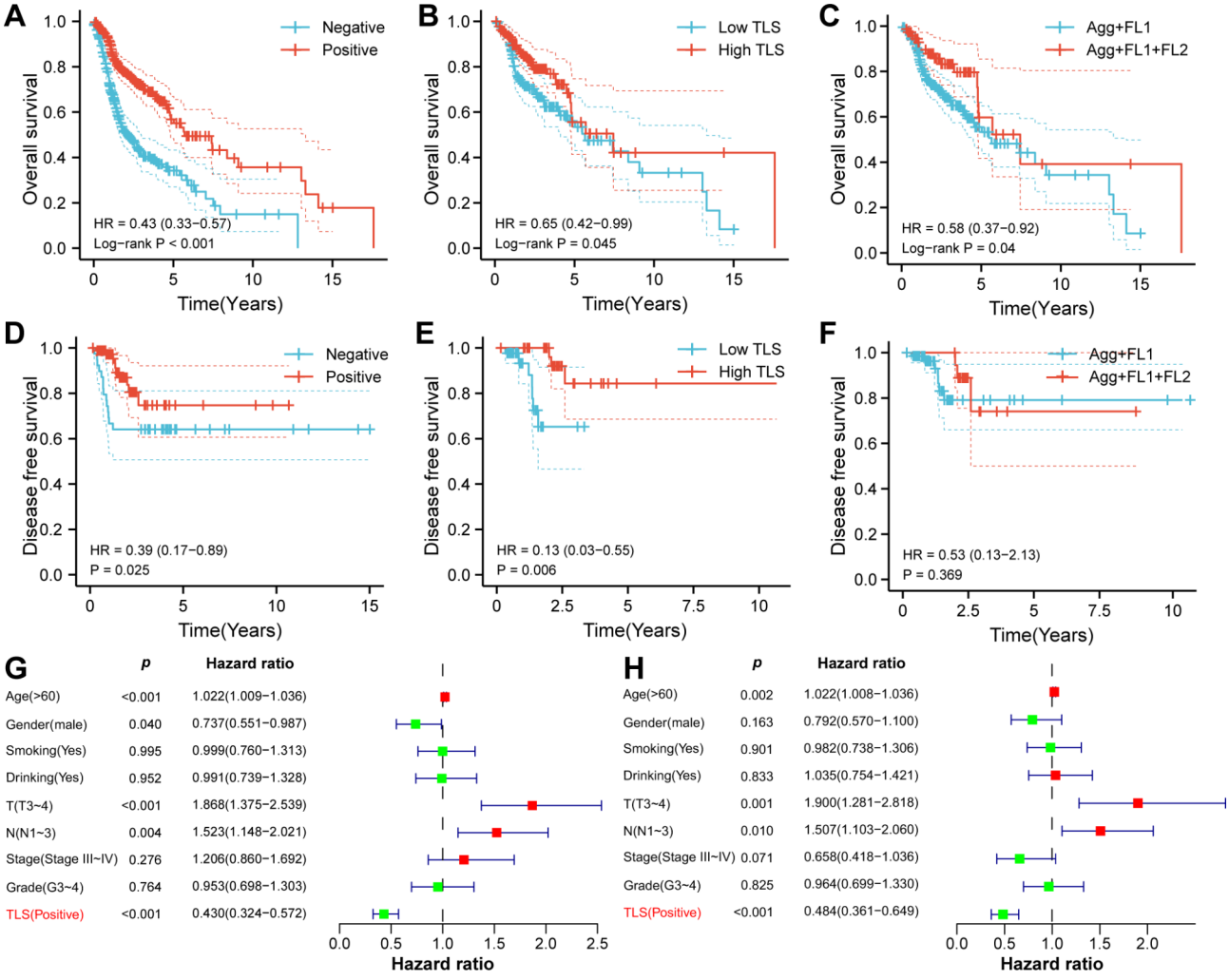

Fig. 2 Impact of TLSs on OS and DFS in patients with OSCC. (**A**, **D**) OS and DFS analyses between the TLS- group and TLS + group. (**B**, **E**) OS and DFS analyses between the low TLS group and high TLS group. (**C**, **F**) OS and DFS analyses between the Agg + FL1 group and Agg + FL1 + FL2 group. **G**, **H** Univariate analysis (**G**) and multivariate analysis (**H**) of TLSs and clinicopathological parameters in the TCGA cohort

improved OS (Fig. 5A, B), while the high expression of CD86 indicated a poor prognosis (Fig. 5C). Second, we investigated the relationships between the clinical parameters and the expression levels of the three TLSRGs. Our findings revealed a significant correlation between the downregulation of CCR7 ($p = 0.036$) and CXCR5 ($p = 0.0051$), alongside the upregulation of CD86 ($p = 0.018$), with the incidence of positive lymph node metastasis (Fig. 5D-F). In addition, CCR7 expression was closely related to the pT classification ($p = 0.00059$), pTNM classification ($p = 0.002$), NES ($p = 0.041$), and PNI ($p = 0.025$) (Fig. 5D; Additional Fig. 1A). Additionally, observable disparities in CD86 expression were noted across varying grade ($p = 0.043$) and PNI groups ($p = 0.0026$) (Fig. 5F; Additional Fig. 1C). We employed a heatmap to delineate the relationships between the risk score and various clinical parameters. This visual representation revealed a significant association between the high-risk group and pT classification, pTNM stage, PNI, NES, and lymph node metastasis (Fig. 5G). The above results indicated that the three TLSRGs were closely related to lymph node metastasis and the prognostic model exhibited favorable predictive ability.

Correlations of TLSs, risk score, and tumor-infiltrating immune cells

Given the crucial role of TLSs in antitumor immunity, TIMER2.0 was utilized to investigate the characteristics of immune cell infiltration in the TLS + OSCC group. As shown in Fig. 6A, strong correlations are noted between TLSs and B cells, CD4 + T cells, CD8 + T cells, and macrophages in OSCC. A high ratio of TLS area suggested abundant B cell, CD4 + T cell, and macrophage infiltration in the microenvironment (Fig. 6B). The infiltration of CD4 + T cells, CD8 + T

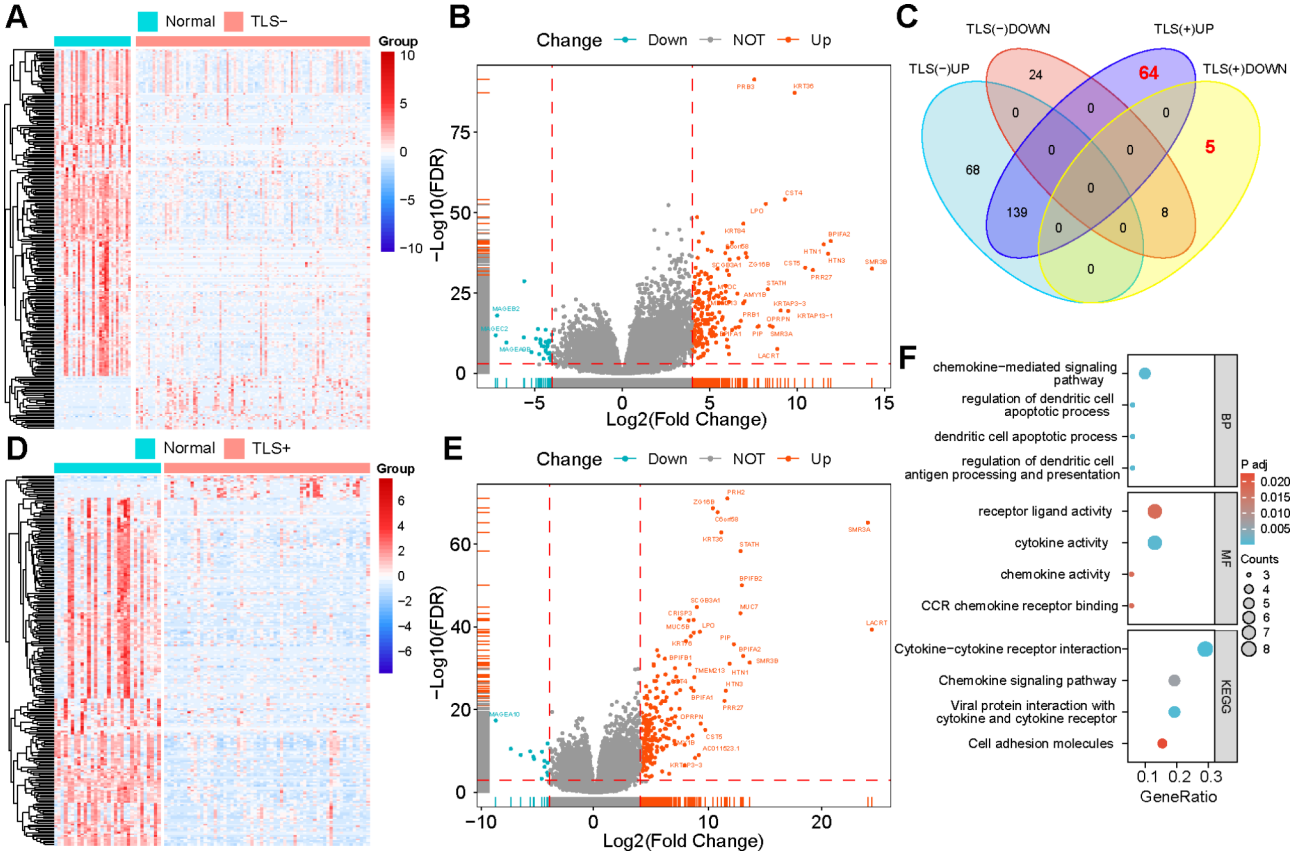

Fig. 3 DEGs and functional analyses. (**A**, **B**) Heatmap (**A**) and volcano map (**B**) of DEGs between the TLS- OSCC group and the normal group. (**D**, **E**) Heatmap (**D**) and volcano map (**E**) of DEGs between the TLS + OSCC group and the normal group. (**C**) Venn diagram of 69 identified TLSRGs. (**F**) GO and KEGG analyses

cells, and macrophages exhibited a negative correlation with the risk score (Fig. 6C), indicating a potential inverse relation between immune cell presence and risk assessment metrics. These results suggested that these three immune cell types played important roles in the formation of TLSs and bolstered anti-tumor defenses.

Establishment of the prognostic nomogram for individualized evaluation

Immunohistochemistry was used to investigate the expression of the characteristic proteins corresponding to the three TLSRGs in clinical samples (Fig. 7A). The result showed that the percentage of CD86-positive cells was the lowest in the TLS + OSCC group (Fig. 7D). Compared with those in the normal group and TLS- OSCC group, the percentages of cells positive for CCR7 and CXCR5 were greater in TLS + OSCC group (Fig. 7B, C).

To further provide reliable prognostic information tailored to individual patients, a predictive nomogram was developed to estimate the survival rates at one, three, and five years for OSCC patients (Fig. 8A). Additionally, a calibration plot was generated to illustrate the model's good predictive value, depicting the predicted probabilities at 1, 3, and 5 years relative to the actual observations (Fig. 8B). The C-index of this model was provided in Additional Table 3.

Discussion

In this study, we analyzed HE-stained WSIs for the detection of TLSs by employing the CNN. Our findings validated TLSs as the robust, independent prognostic marker for OSCC patients. To make TLSs broadly applicable in clinical settings, we developed a risk score model including three TLSRGs and verified its independent prognostic value. We also investigated the relationships between TLSs, risk score, and immune cell infiltration. After verifying the protein expression of the three TLSRGs in clinical samples, a nomogram model was constructed for the individualized evaluation of OSCC patients by incorporating routine clinical metrics.

We found that TLSs were unevenly distributed in OSCC, with its area less than 2.8% of the tumor area. However, in a few cases, the proportion could reach

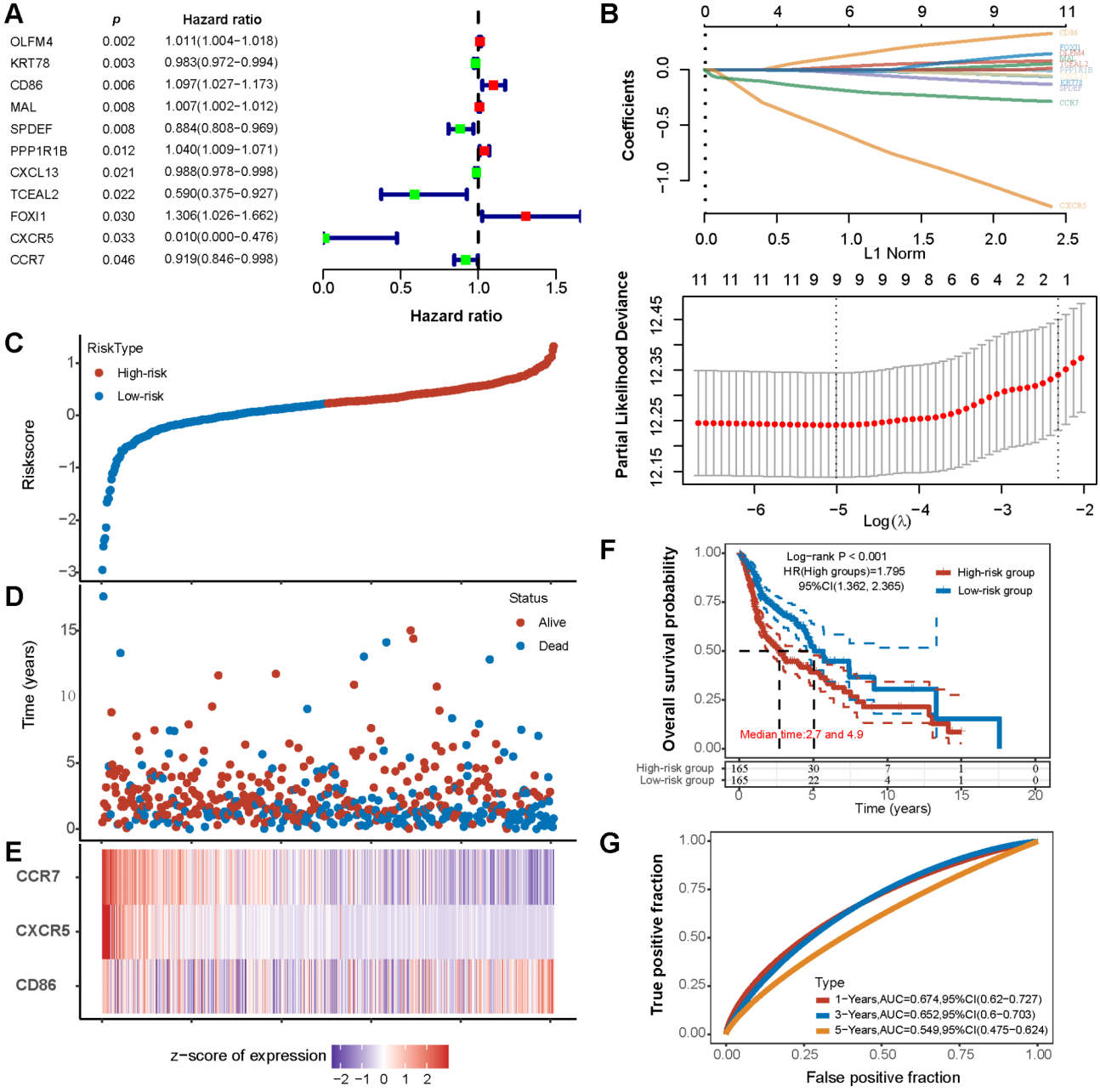

Fig. 4 Establishment of the three-gene risk score model. (**A**) Eleven TLSRGs strongly associated with the OS of OSCC patients. (**B**) The optimal result for 11 TLSRGs according to LASSO regression. In the upper plot, each curve represents the change trajectory of the coefficient of each variable. L1 Norm representing the sum of the absolute values of all nonzero coefficients, and the upper X-axis represents the number of nonzero coefficients in the model. In the lower plot, the upper X-axis represents the number of variables remaining in the equation for different λ. The Y-axis represents the partial likelihood deviance, and a smaller Y value indicates a better fit of the equation. The vertical dotted lines are drawn at the optimal values using the minimum (left) and 1-SE criteria(right). (**C**) The distribution of risk score in OSCC patients. (**D**) Survival status according to the risk score. (**E**) Heatmap of the three TLSRGs in the high- and low-risk groups. (**F**) K-M plot of OSCC patients in the low- and high-risk groups. (**G**) ROC analysis of the risk score model predicted OS. AUC: area under the curve

Table 2 Three key TLSRGs were selected after step Cox regression analysis

TLSRGs	Coefficient
CD86	0.3169
CXCR5	-1.3345
CCR7	-0.2974

4–6%. This suggests that the patch- or tile-based approaches for image analysis used in many studies are inappropriate, which may lead to misestimation of the presence of TLSs. Zeng et al. [15] reported that the percentage of TLS-positive breast ductal carcinomas was 24.7%, which is significantly different from

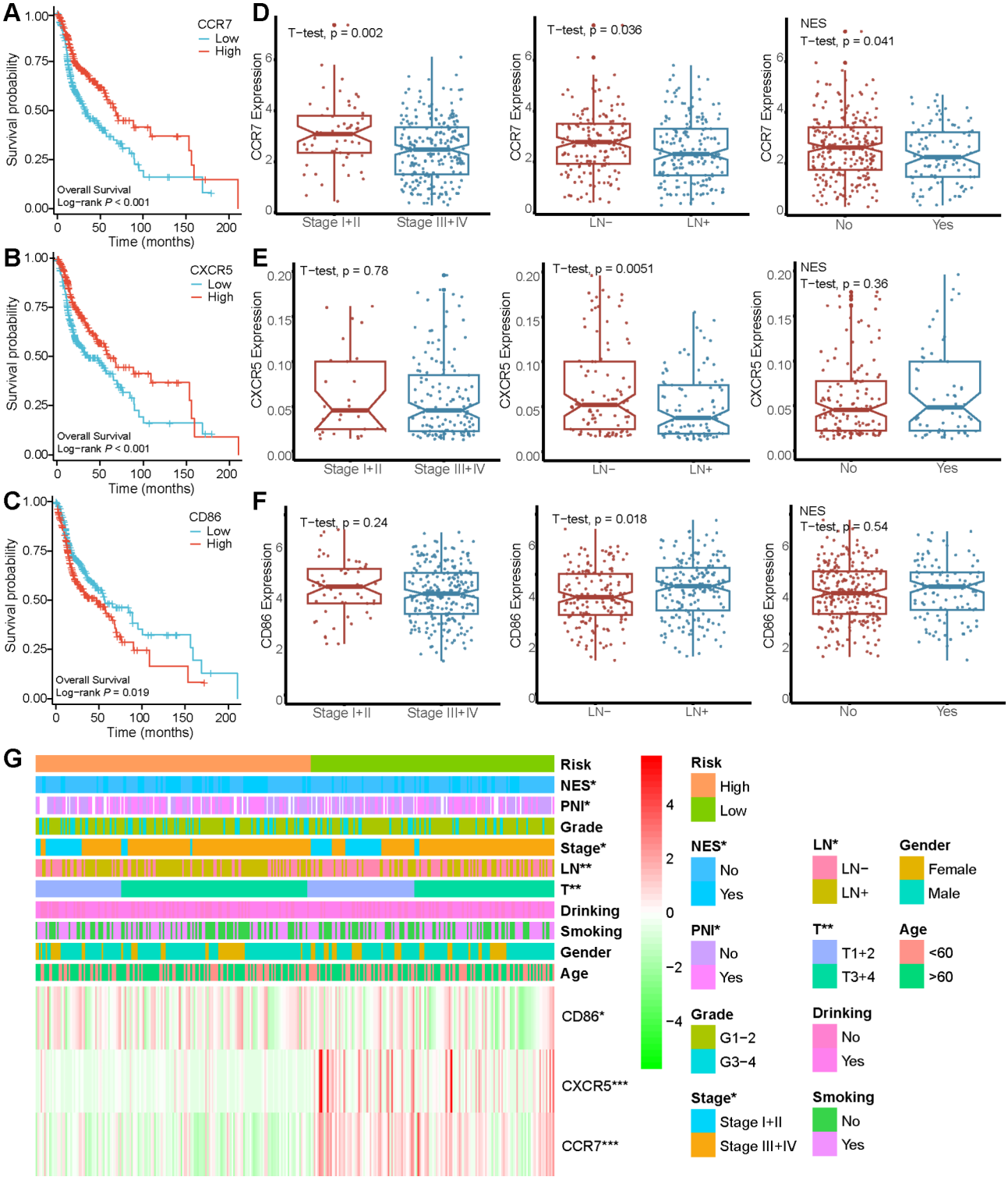

Fig. 5 Correlations between the prognostic model and clinical data. (**A-C**) K-M plots of OSCC patients in groups with different expression levels of the three TLSRGs. (**D-G**) Correlations between the expression levels of CCR7, CXCR5, CD86, risk score, and clinical parameters. LN+, positive lymph node metastasis; LN-, no lymph node metastasis

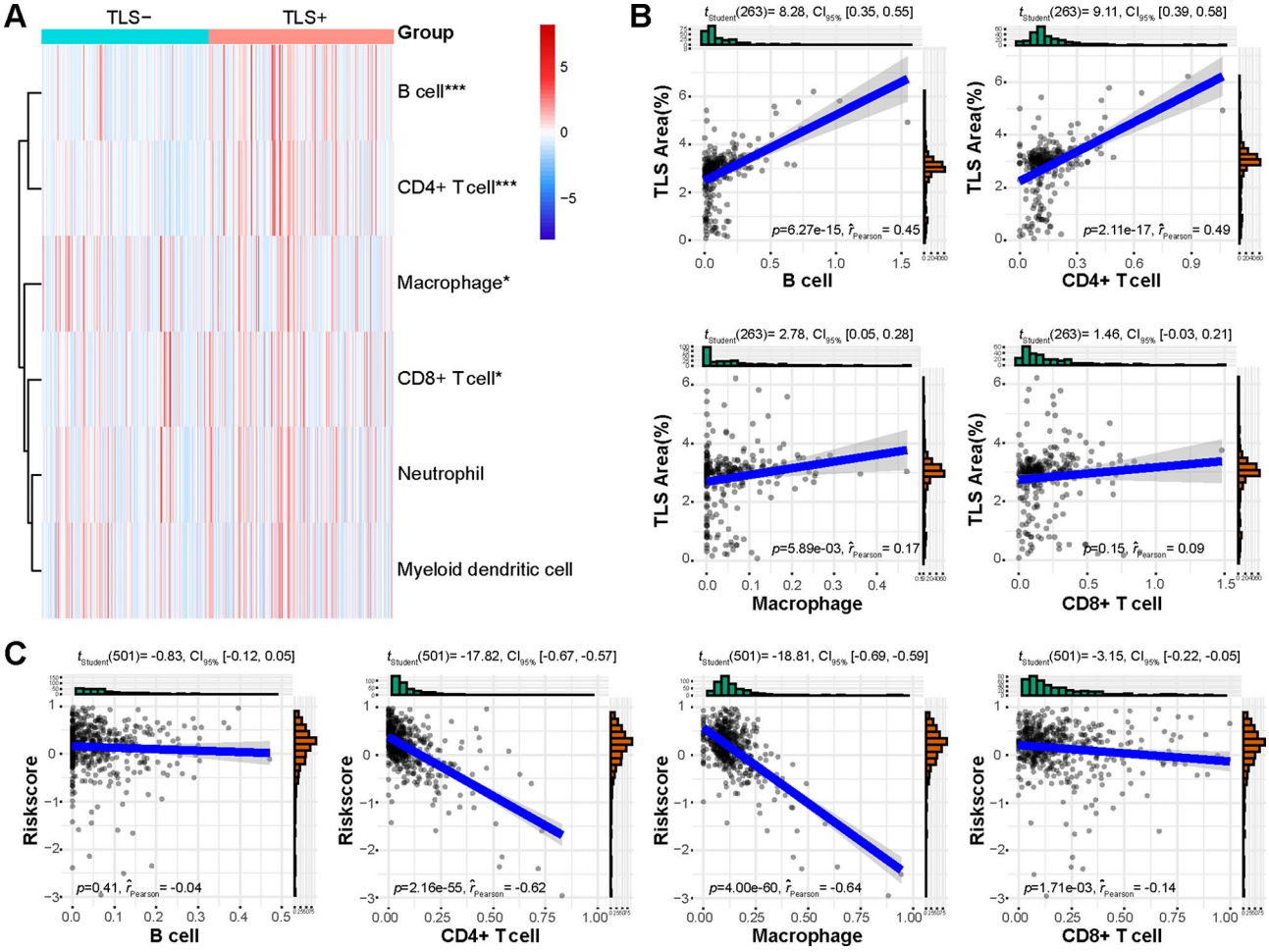

Fig. 6 Correlations between TLSs, risk score, and immune cell infiltration. (**A**) Comparison of the abundance of infiltrating immune cells in the TLS + and TLS- groups. (**B**) Correlation between the ratio of the TLS area and immune cell infiltration. (**C**) Correlation between the risk score and immune cell infiltration

the 60.3% reported in a Korean study [35]. Wirsing's study revealed that analyzing a single level in OSCC tissue blocks failed to detect approximately one-third of TLS + patients [36]. Most previous studies have used multiplex immunohistochemistry (mIHC) or immunofluorescence (mIF) approaches to detect TLSs [37, 38]. Despite the potential of mIHC and mIF approaches for providing detailed cellular insights, their adoption in clinical settings is restricted by their prohibitive costs and operational complexity. Conversely, HE staining stands as the cornerstone of histopathological analysis due to its affordability and widespread availability, offering a practical alternative for routine examinations. TLSs vary greatly in size, density, maturity, and distribution, and the evaluation of TLSs is affected by pathologists' experience [39, 40]. Manual assessment is labor-intensive, relies on expertise, and often yields poor reproducibility. Therefore, we believe that it is more reliable and standardized to use the CNN to identify TLSs on HE-stained WSIs at multiple levels.

Research indicates that the presence of mature TLSs is positively correlated with enhanced OS and DFS among patients with early-stage OTSCC [20]. OSCC patients without TLSs have a poorer prognosis than those with TLSs [21]. Similarly, we found that the presence of TLSs was a positive factor for OS and DFS and was an independent prognostic factor for OSCC. OSCC patients with FL2 generally had longer overall survival than those without FL2, but there was no significant difference in DFS between the two groups. In OSCC, the predictive value of the TLS area ratio is better than that of maturity. Patients with a high TLS area have a favorable prognosis.

Despite these advancements, validated molecular markers linked to TLSs that can consistently predict the prognosis of OSCC patients are lacking. Through a comparison of sequencing data from TLS + and TLS- OSCC tissues, we identified 69 TLSRGs, which were mainly enriched in the chemokine-mediated signaling pathway, regulation of dendritic cell antigen processing

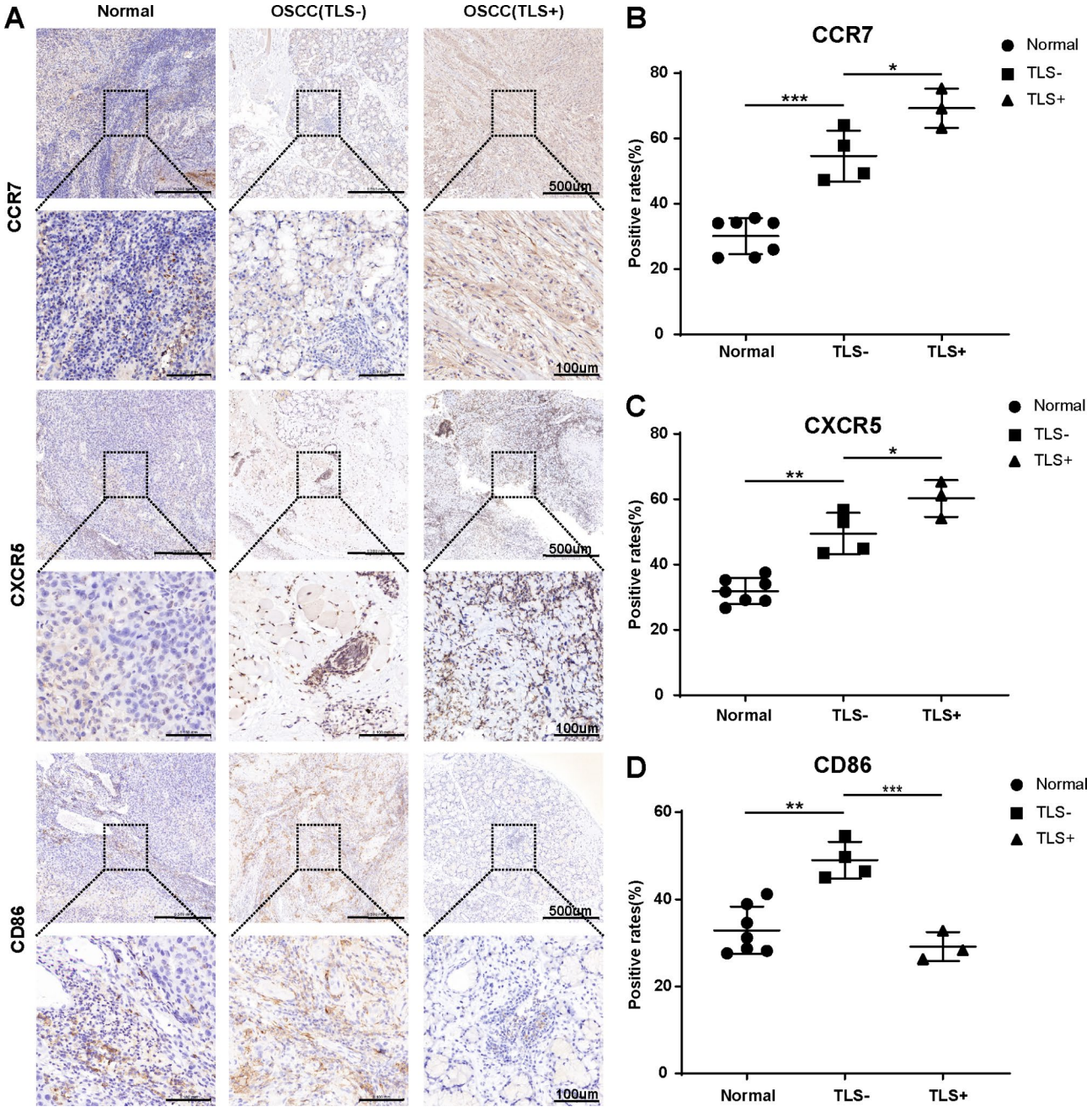

Fig. 7 The protein expression of three TLSRGs in clinical samples. (**A**) Immunohistochemical results of CCR7, CXCR5, and CD86 in the normal group, TLS- OSCC group, and TLS + OSCC group. (**B-D**) The percentage of CCR7-, CXCR5-, CD86-positive cells in the normal group, TLS- OSCC group, and TLS + OSCC group

and presentation, and cytokine-cytokine receptor interaction. Based on the abundance of chemokines and cytokines expressed in TLSs, some studies have established the disease-specific gene signatures to assess the presence of TLSs in tumors [14, 27]. Liu et al. [19] propose a 13-gene signature to assess the level of TLSs in HNSCC and these selected genes partially overlap with our screening results. In our research, CCR7, CXCR5, and CD86 were identified by LASSO regression and stepwise Cox regression analysis, and a prognostic model was constructed.

CXCR5 and CCR7 play pivotal roles in lymphoid organogenesis and the preservation of lymphoid tissue architecture, orchestrating the migration of lymphocytes and dendritic cells (DCs) to secondary lymphoid structures [41]. CCR7 is highly expressed on some CD4 + T cells, B cells, and DCs, which migrate to the T-cell zone via CCL19 and CCL21. DCs introduce

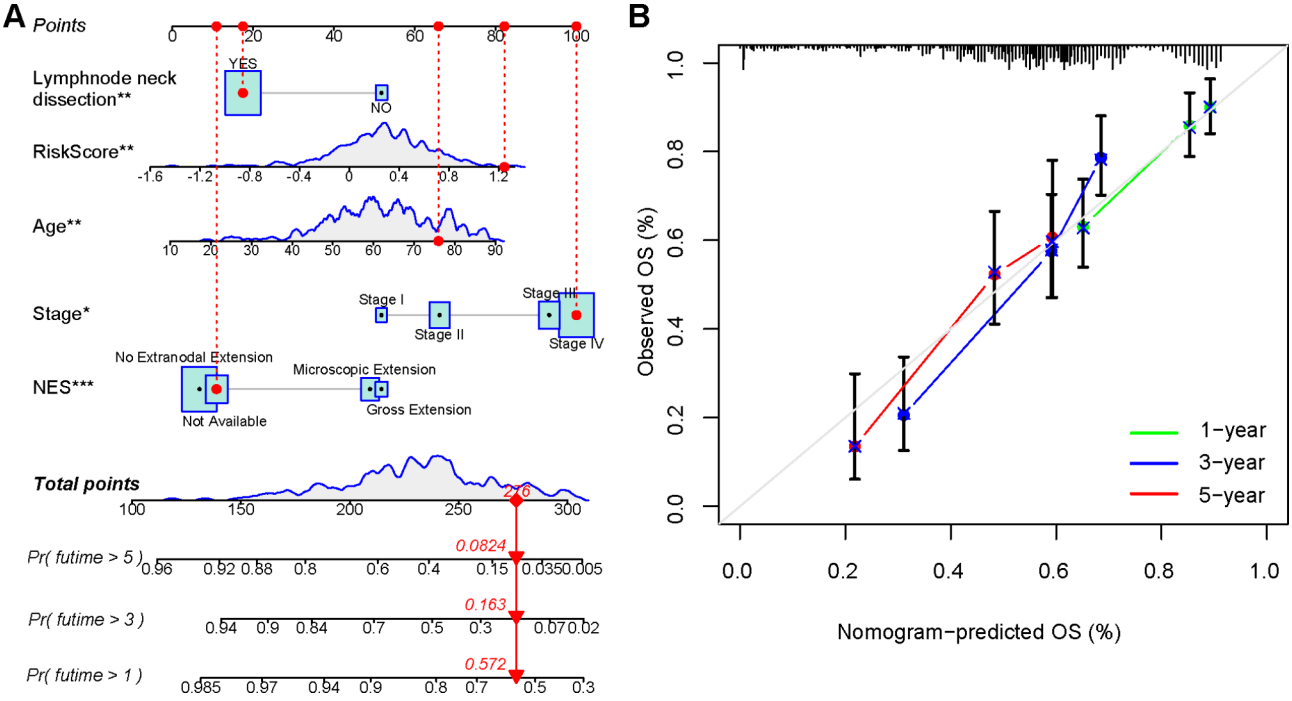

Fig. 8 Establishment of the prognostic nomogram model. (**A**) The nomogram model. Left, key variables affecting the prognosis; top, Points represent the value range of the variables; bottom, Total points represent the total score of the corresponding individual scores added after all variables are valued. The Pr(futime > 5) indicates that the 5-year survival probability predicted from the patient's total score (276) is 0.0824. (**B**) Calibration curve of the nomogram model

antigens to uninitiated T cells, facilitating the transformation of naive CD4 + T cells into follicular helper T cells (Tfh cells), which are essential for adaptive immunity [42]. The expression of the chemokine receptor CXCR5 on Tfh cells gradually increases, and the expression of CCR7 decreases [43].

CXCR5, which is predominantly expressed on B cells, Tfh cells, and mature DCs, plays a crucial role in cell migration [44–46]. Its likely sole ligand, CXCL13, is expressed by follicular dendritic cells (FDCs) and various stromal cells situated in the B-cell regions of secondary lymphoid organs [47, 48]. Tfh cells and B cells with high CXCR5 expression migrate to the B-cell zone through CXCL13 [43]. B cells and Tfh cells engage with FDCs to foster the germinal center reaction, which leads to the evolution of B cells into memory B cells and enduring plasma cells [49]. TLSs are structurally and functionally similar to secondary lymphoid organs [6] and are the site of effector T cell, memory T cell as well as B cell differentiation [50]. Therefore, we hypothesize that CXCR5 and CCR7 play similar roles in TLSs, such as recruiting immune cells and promoting TLSs formation.

Primarily located on antigen-presenting cells, CD86 serves as a crucial ligand for CD28 and CTLA-4, which are found on the surface of T cells [51]. The interaction of CD86 with CD28 stimulates T cell activation, while the interaction of CD86 with CTLA-4 suppresses T cell activation and decreases the immune response [52, 53]. According to previous studies, CTLA-4 has a greater binding affinity for CD86 than for CD28, and the CTLA-4-CD86 interaction counteracts the CD86-CD28 interaction, leading to immune suppression [54, 55].

Our research revealed a significant correlation between TLSs and the presence of B cells, CD4 + T cells, CD8 + T cells, and macrophages in OSCC, highlighting their potential role in the tumor microenvironment. A rise in the percentage of TLS area was favorably connected with immune cell infiltration, although it was adversely correlated with the risk score. The upregulation of CCR7 and CXCR5 and the downregulation of CD86 and the risk score were negatively correlated with lymph node metastasis, indicating a better prognosis. These findings indicate that the presence of TLSs is negatively correlated with lymph node metastasis and predicts a better prognostic outcome. Our findings are supported by other literature. According to the Human Protein Atlas [56], high CCR7 expression is associated with a better prognosis in OSCC patients [57]. In melanoma, CCR7 + DCs play a key role in trafficking tumor antigens to lymphoid tissues and activating T cells [58]. Zhang et al. reported that CXCR5 + CD4 + Tfh cells

play a pivotal role in developing and sustaining TLSs and are associated with a good prognosis in HNSCC patients [16]. Wang et al. confirmed that high levels of CXCR5 + CD8 + T cells correlate with improved OS in gastric cancer patients [59]. Upregulation of CTLA4 is an important immunosuppressive mechanism in HNSCC [60]. Wakasu and Zhang et al. reported that patients with mature TLSs have a significantly lower incidence of lymph node metastasis [12, 61].

We propose that TLSs distributed in tumors are on the front line of antitumor immunity. A high TLS area ratio and maturity indicate strong antitumor immunity. When the strength of antitumor immunity around highly malignant tumors is weak, the incidence of lymph node metastasis is greatly increased. However, some studies suggest that cancer cells can metastasize to lymph nodes by upregulating CCR7 expression [62], leading to a worse prognosis [63–65]. Two opposite effects of CCR7 have been reported in different cancer studies, and one possible explanation is that the changes in the tumor microenvironment alter the effect of CCR7. In the early stage of cancer, a small minority of CCR7 + tumor cells migrate to lymph nodes, where they may play a role in presenting tumor antigens and activating immunity. With tumor progression, alterations in the microenvironment may facilitate the colonization of CCR7 + tumor cells in lymph nodes. Second, the heterogeneities of tumors at various sites are large, and the interactions between immune cells and tumors are complex. A single indicator cannot accurately predict the prognosis of all cancers, so it is necessary to combine multiple indicators to make a more accurate prediction. To a certain extent, these findings validate the appropriateness of selecting these three TLSRGs to construct a prognostic model. We further confirmed the prognostic model's effectiveness in clinical applications at the tissue level by performing immunohistochemical staining of three TLSRGs. Finally, routine clinical parameters were integrated into the risk score model, and the nomogram model was constructed to enhance the specificity of individual prognosis prediction.

Our study has several limitations. First, it is important to note that the results primarily rely on the TCGA dataset and require further validation in additional databases. Some individuals had received immune or targeted treatments, which influenced the prognosis analysis. Although the three TLSRGs were validated in clinical samples, the biological functions of these genes in OSCC necessitate further verification through experiments, and expanding the sample size would be beneficial.

Conclusions

At present, only a few studies have demonstrated that TLSs can act as the prognostic biomarker and the predictor of immunotherapy efficacy in OSCC patients. Many different markers, which cannot be widely used in clinical practice, have been used to characterize TLSs. Compared to previous studies, this study offers the following advantages: ① it used the CNN to accurately identify TLSs and underscores the potential of integrating advanced image analysis techniques in oncological prognostication; ② it explored the relationships between TLSs, lymph node metastasis, and immune infiltration; and ③ it is the first OSCC nomogram prediction model based on TLSRGs, which can be used as a supplementary indicator of the prognosis in OSCC patients. Its use may be related to further refinement of the current staging system and improvement of risk stratification.

Abbreviations

Agg	Lymphoid aggregates
AUC	Area under the curve
CI	Confidence interval
DCs	Dendritic cells
DEGs	Differentially expressed genes
DFS	Disease-free survival
FDCs	Follicular dendritic cells
FDR	False discovery rate
FL1	Primary follicle-like TLSs
FL2	Secondary follicle-like TLSs
GCO	Global Cancer Observatory
GO	Gene Ontology
HE	Hematoxylin and eosin
HNSCC	Head neck squamous cell carcinoma
HR	Hazard ratio
KEGG	Kyoto Encyclopedia of Genes and Genomes
mIHC	Multiplex immunohistochemistry
mIF	Multiplex immunofluorescence
NES	Nodal extracapsular spread
OTSCC	Oral tongue squamous cell carcinoma
OS	Overall survival
OSCC	Oral squamous cell carcinoma
PNI	Perineural invasion
ROC	Receiver operating characteristic
TCGA	The Cancer Genome Atlas
Tfh cells	Follicular helper T cells
TIMER	Tumor Immune Estimation Resource
TLSs	Tertiary lymphoid structures
TLSRGs	TLS-related genes
TNM stage	Tumor node metastasis stage
WSIs	Whole slide images

Supplementary Information

The online version contains supplementary material available at https://doi.org/10.1186/s12935-024-03543-7.

Additional Figure 1: The correlations between the three TLSRGs and the clinical data in patients with OSCC. (**A**) The correlation between the expression level of CCR7 and the clinical data; (**B**) The correlation between the expression level of CXCR5 and the clinical data; (**C**) The correlation between the expression level of CD86 and the clinical data. NES, nodal extracapsular spread

Additional File 1: The clinicopathological information and TLSs expression in 503 HNSCC patients in the TCGA cohort

Additional File 2: The types of TLSs in OSCC samples

Additional Table 1: Univariate Cox analysis of the 69 prognosis-related TLSRGs

Additional Table 2: TLSs signatures in various tumors

Additional Table 3: Time-dependent internal validation represented by C-index

Acknowledgements
Not applicable.

Author contributions
BS and FZ designed the study. CG and FZ performed the bioinformatics analyses. YT and QX contributed to the clinical sample collection and experiments. BS wrote the manuscript, and KW helped to revise the manuscript. All the authors have read and approved the final manuscript.

Funding
This study was supported by the National Engineering Research Center of Oral Biomaterials and Digital Medical Devices of Peking University and Hospital of Stomatology (PKUSS20230202), the Department of Science and Technology of Hunan Province (2023JJ41028, 2024JJ6352), and the Natural Science Foundation of Hainan Province (821MS132).

Data availability
Data is provided within the manuscript or supplementary information files.

Declarations

Ethics approval and consent to participate
This study received approval from the Ethics Committee of the Second Xiangya Hospital of Central South University (No.2022111194), and all participants provided informed consent prior to their inclusion.

Consent for publication
Not applicable.

Competing interests
The authors declare no competing interests.

Author details
[1]Department of Oral and Maxillofacial Surgery, Center of Stomatology, Xiangya Hospital, Central South University, Changsha, Hunan, P. R. China
[2]Research Center of Oral and Maxillofacial Tumor, Xiangya Hospital, Central South University, Changsha, Hunan, P. R. China
[3]Institute of Oral Cancer and Precancerous Lesions, Central South University, Changsha, Hunan, P. R. China
[4]National Engineering Research Center of Oral Biomaterials and Digital Medical Devices, Peking University School and Hospital of Stomatology, Beijing, P. R. China
[5]Department of Oral Maxillofacial Surgery, Hainan General Hospital, Haikou, Hainan, P. R. China
[6]Department of Nursing, The Second Affiliated Hospital of Hunan University of Chinese Medicine, Changsha, Hunan, P. R. China
[7]Department of Oral and Maxillofacial Surgery, The Second Xiangya Hospital of Central South University, Changsha, Hunan, P. R. China
[8]Xiangya Stomatological Hospital & Xiangya School of Stomatology, Central South University, Changsha, Hunan, P. R. China

Received: 2 May 2024 / Accepted: 21 October 2024
Published online: 26 October 2024

References

1. Tan Y, Wang Z, Xu M, Li B, Huang Z, Qin S, et al. Oral squamous cell carcinomas: state of the field and emerging directions. Int J Oral Sci. 2023;15(1):44.
2. Mody MD, Rocco JW, Yom SS, Haddad RI, Saba NF. Head and neck cancer. Lancet. 2021;398(10318):2289–99.
3. Amin MB, Greene FL, Edge SB, Compton CC, Gershenwald JE, Brookland RK, et al. The Eighth Edition AJCC Cancer staging Manual: continuing to build a bridge from a population-based to a more personalized approach to cancer staging. CA Cancer J Clin. 2017;67(2):93–9.
4. Zhang SY, Ren XY, Wang CY, Chen XJ, Cao RY, Liu Q, et al. Comprehensive characterization of Immune Landscape based on Epithelial-Mesenchymal Transition Signature in OSCC: implication for prognosis and immunotherapy. Front Oncol. 2021;11:587862.
5. Balachandran VP, Gonen M, Smith JJ, DeMatteo RP. Nomograms in oncology: more than meets the eye. Lancet Oncol. 2015;16(4):e173–80.
6. Pitzalis C, Jones GW, Bombardieri M, Jones SA. Ectopic lymphoid-like structures in infection, cancer and autoimmunity. Nat Rev Immunol. 2014;14(7):447–62.
7. Schumacher TN, Thommen DS. Tertiary lymphoid structures in cancer. Science. 2022;375(6576):eabf9419.
8. Zhao Z, Ding H, Lin ZB, Qiu SH, Zhang YR, Guo YG, et al. Relationship between Tertiary Lymphoid structure and the prognosis and clinicopathologic characteristics in solid tumors. Int J Med Sci. 2021;18(11):2327–38.
9. Shang T, Jiang T, Lu T, Wang H, Cui X, Pan Y, et al. Tertiary lymphoid structures predict the prognosis and immunotherapy response of cholangiocarcinoma. Front Immunol. 2023;14:1166497.
10. Cabrita R, Lauss M, Sanna A, Donia M, Skaarup Larsen M, Mitra S, et al. Tertiary lymphoid structures improve immunotherapy and survival in melanoma. Nature. 2020;577(7791):561–5.
11. Hayashi Y, Makino T, Sato E, Ohshima K, Nogi Y, Kanemura T, et al. Density and maturity of peritumoral tertiary lymphoid structures in oesophageal squamous cell carcinoma predicts patient survival and response to immune checkpoint inhibitors. Br J Cancer. 2023;128(12):2175–85.
12. Zhang C, Wang XY, Zuo JL, Wang XF, Feng XW, Zhang B et al. Localization and density of tertiary lymphoid structures associate with molecular subtype and clinical outcome in colorectal cancer liver metastases. J Immunother Cancer. 2023;11(2).
13. Wang Q, Sun K, Liu R, Song Y, Lv Y, Bi P, et al. Single-cell transcriptome sequencing of B-cell heterogeneity and tertiary lymphoid structure predicts breast cancer prognosis and neoadjuvant therapy efficacy. Clin Transl Med. 2023;13(8):e1346.
14. Xu W, Ma C, Liu W, Anwaier A, Tian X, Shi G, et al. Prognostic value, DNA variation and immunologic features of a tertiary lymphoid structure-related chemokine signature in clear cell renal cell carcinoma. Cancer Immunol Immunother. 2022;71(8):1923–35.
15. Zeng L, Koh VCY, Chen XY, Tan PH. Tertiary lymphoid structures in breast ductal carcinoma in situ correlate with adverse pathological parameters. Histopathology. 2023;82(5):779–88.
16. Zhang B, Li H, Liu YT, Xiong D, Zhang L, Sun ZJ. Single-cell chemokine receptor profiles delineate the immune contexture of tertiary lymphoid structures in head and neck squamous cell carcinoma. Cancer Lett. 2023;558:216105.
17. Badalamenti G, Fanale D, Incorvaia L, Barraco N, Listì A, Maragliano R, et al. Role of tumor-infiltrating lymphocytes in patients with solid tumors: can a drop dig a stone? Cell Immunol. 2019;343:103753.
18. Sautès-Fridman C, Petitprez F, Calderaro J, Fridman WH. Tertiary lymphoid structures in the era of cancer immunotherapy. Nat Rev Cancer. 2019;19(6):307–25.
19. Liu Z, Meng X, Tang X, Zou W, He Y. Intratumoral tertiary lymphoid structures promote patient survival and immunotherapy response in head neck squamous cell carcinoma. Cancer Immunol Immunother. 2022.
20. Wang C, Huang Z, Zhang M, Xiong G, Chen X, Xie N. Prognostic value of tertiary lymphoid structures in early clinical stage oral tongue squamous cell carcinoma. J Oral Pathol Med. 2021;50(8):776–84.
21. Li Q, Liu X, Wang D, Wang Y, Lu H, Wen S, et al. Prognostic value of tertiary lymphoid structure and tumour infiltrating lymphocytes in oral squamous cell carcinoma. Int J Oral Sci. 2020;12(1):24.
22. Barmpoutis P, Di Capite M, Kayhanian H, Waddingham W, Alexander DC, Jansen M, et al. Tertiary lymphoid structures (TLS) identification and density assessment on H&E-stained digital slides of lung cancer. PLoS ONE. 2021;16(9):e0256907.
23. Weinstein JN, Collisson EA, Mills GB, Shaw KR, Ozenberger BA, Ellrott K, et al. The Cancer Genome Atlas Pan-cancer analysis project. Nat Genet. 2013;45(10):1113–20.

24. Gutman DA, Cobb J, Somanna D, Park Y, Wang F, Kurc T, et al. Cancer Digital Slide Archive: an informatics resource to support integrated in silico analysis of TCGA pathology data. J Am Med Inf Assoc. 2013;20(6):1091–8.
25. Chen L-C, Zhu Y, Papandreou G, Schroff F, Adam H, editors. Encoder-decoder with Atrous Separable Convolution for Semantic Image Segmentation. Computer vision – ECCV 2018; 2018 2018//; Cham: Springer International Publishing.
26. Tang W, Zou D, Yang S, Shi J, Dan J, Song G. A two-stage approach for automatic liver segmentation with faster R-CNN and DeepLab. Neural Comput Appl. 2020;32(11):6769–78.
27. Finkin S, Yuan D, Stein I, Taniguchi K, Weber A, Unger K, et al. Ectopic lymphoid structures function as microniches for tumor progenitor cells in hepatocellular carcinoma. Nat Immunol. 2015;16(12):1235–44.
28. Murakami J, Shimizu Y, Kashii Y, Kato T, Minemura M, Okada K, et al. Functional B-cell response in intrahepatic lymphoid follicles in chronic hepatitis C. Hepatology. 1999;30(1):143–50.
29. Kolde Rpheatmap. Pretty Heatmaps. R package version 1.0.12. 2019 [https://CRAN.R-project.org/package=pheatmap
30. Ashburner M, Ball CA, Blake JA, Botstein D, Butler H, Cherry JM, et al. Gene ontology: tool for the unification of biology. The Gene Ontology Consortium. Nat Genet. 2000;25(1):25–9.
31. Kanehisa M, Sato Y, Kawashima M, Furumichi M, Tanabe M. KEGG as a reference resource for gene and protein annotation. Nucleic Acids Res. 2016;44(D1):D457–62.
32. Wu T, Hu E, Xu S, Chen M, Guo P, Dai Z, et al. clusterProfiler 4.0: a universal enrichment tool for interpreting omics data. Innov (Camb). 2021;2(3):100141.
33. Heagerty PJ, Zheng Y. Survival model predictive accuracy and ROC curves. Biometrics. 2005;61(1):92–105.
34. Li T, Fan J, Wang B, Traugh N, Chen Q, Liu JS, et al. TIMER: a web server for Comprehensive Analysis of Tumor-infiltrating Immune cells. Cancer Res. 2017;77(21):e108–10.
35. Kim A, Heo SH, Kim YA, Gong G, Jin Lee H. An examination of the Local Cellular Immune Response to examples of both ductal carcinoma in situ (DCIS) of the breast and DCIS with Microinvasion, with emphasis on Tertiary lymphoid structures and Tumor infiltrating Lymphoctytes. Am J Clin Pathol. 2016;146(1):137–44.
36. Wirsing AM, Rikardsen OG, Steigen SE, Uhlin-Hansen L, Hadler-Olsen E. Characterisation and prognostic value of tertiary lymphoid structures in oral squamous cell carcinoma. BMC Clin Pathol. 2014;14:38.
37. Ruffin AT, Cillo AR, Tabib T, Liu A, Onkar S, Kunning SR, et al. B cell signatures and tertiary lymphoid structures contribute to outcome in head and neck squamous cell carcinoma. Nat Commun. 2021;12(1):3349.
38. Rakaee M, Kilvaer TK, Jamaly S, Berg T, Paulsen EE, Berglund M, et al. Tertiary lymphoid structure score: a promising approach to refine the TNM staging in resected non-small cell lung cancer. Br J Cancer. 2021;124(10):1680–9.
39. Díaz A, Forner A. Prognosis assessment by pathologist: is the detection of intratumoural tertiary lymphoid structures a reliable tool? J Hepatol. 2019;70(1):11–2.
40. Munoz-Erazo L, Rhodes JL, Marion VC, Kemp RA. Tertiary lymphoid structures in cancer - considerations for patient prognosis. Cell Mol Immunol. 2020;17(6):570–5.
41. Müller G, Höpken UE, Lipp M. The impact of CCR7 and CXCR5 on lymphoid organ development and systemic immunity. Immunol Rev. 2003;195:117–35.
42. Barnett LG, Simkins HM, Barnett BE, Korn LL, Johnson AL, Wherry EJ, et al. B cell antigen presentation in the initiation of follicular helper T cell and germinal center differentiation. J Immunol. 2014;192(8):3607–17.
43. Allen CD, Cyster JG. Follicular dendritic cell networks of primary follicles and germinal centers: phenotype and function. Semin Immunol. 2008;20(1):14–25.
44. Bindea G, Mlecnik B, Tosolini M, Kirilovsky A, Waldner M, Obenauf AC, et al. Spatiotemporal dynamics of intratumoral immune cells reveal the immune landscape in human cancer. Immunity. 2013;39(4):782–95.
45. Garg R, Blando JM, Perez CJ, Abba MC, Benavides F, Kazanietz MG. Protein Kinase C Epsilon Cooperates with PTEN loss for prostate tumorigenesis through the CXCL13-CXCR5 pathway. Cell Rep. 2017;19(2):375–88.
46. Gu-Trantien C, Migliori E, Buisseret L, de Wind A, Brohée S, Garaud S et al. CXCL13-producing TFH cells link immune suppression and adaptive memory in human breast cancer. JCI Insight. 2017;2(11).
47. Gunn MD, Ngo VN, Ansel KM, Ekland EH, Cyster JG, Williams LT. A B-cell-homing chemokine made in lymphoid follicles activates Burkitt's lymphoma receptor-1. Nature. 1998;391(6669):799–803.
48. Ansel KM, Ngo VN, Hyman PL, Luther SA, Förster R, Sedgwick JD, et al. A chemokine-driven positive feedback loop organizes lymphoid follicles. Nature. 2000;406(6793):309–14.
49. Tokunaga R, Naseem M, Lo JH, Battaglin F, Soni S, Puccini A, et al. B cell and B cell-related pathways for novel cancer treatments. Cancer Treat Rev. 2019;73:10–9.
50. Germain C, Gnjatic S, Tamzalit F, Knockaert S, Remark R, Goc J, et al. Presence of B cells in tertiary lymphoid structures is associated with a protective immunity in patients with lung cancer. Am J Respir Crit Care Med. 2014;189(7):832–44.
51. Bugeon L, Dallman MJ. Costimulation of T cells. Am J Respir Crit Care Med. 2000;162(4 Pt 2):S164–8.
52. Bolandi N, Derakhshani A, Hemmat N, Baghbanzadeh A, Asadzadeh Z, Afrashteh Nour M, et al. The positive and negative Immunoregulatory Role of B7 Family: promising novel targets in gastric Cancer treatment. Int J Mol Sci. 2021;22:19.
53. Romo-Tena J, Gómez-Martín D, Alcocer-Varela J. CTLA-4 and autoimmunity: new insights into the dual regulator of tolerance. Autoimmun Rev. 2013;12(12):1171–6.
54. Krummel MF, Allison JP. CD28 and CTLA-4 have opposing effects on the response of T cells to stimulation. J Exp Med. 1995;182(2):459–65.
55. Chikuma S. CTLA-4, an essential Immune-Checkpoint for T-Cell activation. Curr Top Microbiol Immunol. 2017;410:99–126.
56. Uhlen M, Zhang C, Lee S, Sjöstedt E, Fagerberg L, Bidkhori G, et al. A pathology atlas of the human cancer transcriptome. Science. 2017;357:6352.
57. Korbecki J, Grochans S, Gutowska I, Barczak K, Baranowska-Bosiacka I. CC chemokines in a Tumor: a review of Pro-cancer and Anti-cancer properties of receptors CCR5, CCR6, CCR7, CCR8, CCR9, and CCR10 ligands. Int J Mol Sci. 2020;21(20).
58. Roberts EW, Broz ML, Binnewies M, Headley MB, Nelson AE, Wolf DM, et al. Critical role for CD103(+)/CD141(+) dendritic cells bearing CCR7 for Tumor Antigen Trafficking and priming of T cell immunity in Melanoma. Cancer Cell. 2016;30(2):324–36.
59. Wang J, Li R, Cao Y, Gu Y, Fang H, Fei Y, et al. Intratumoral CXCR5(+)CD8(+)T associates with favorable clinical outcomes and immunogenic contexture in gastric cancer. Nat Commun. 2021;12(1):3080.
60. Yu GT, Bu LL, Zhao YY, Mao L, Deng WW, Wu TF, et al. CTLA4 blockade reduces immature myeloid cells in head and neck squamous cell carcinoma. Oncoimmunology. 2016;5(6):e1151594.
61. Wakasu S, Tagawa T, Haratake N, Kinoshita F, Oku Y, Ono Y, et al. Preventive effect of tertiary lymphoid structures on lymph node metastasis of lung adenocarcinoma. Cancer Immunol Immunother. 2023;72(6):1823–34.
62. Morein D, Erlichman N, Ben-Baruch A. Beyond cell motility: the expanding roles of chemokines and their receptors in Malignancy. Front Immunol. 2020;11:952.
63. Sperveslage J, Frank S, Heneweer C, Egberts J, Schniewind B, Buchholz M, et al. Lack of CCR7 expression is rate limiting for lymphatic spread of pancreatic ductal adenocarcinoma. Int J Cancer. 2012;131(4):E371–81.
64. Ding Y, Shimada Y, Maeda M, Kawabe A, Kaganoi J, Komoto I, et al. Association of CC chemokine receptor 7 with lymph node metastasis of esophageal squamous cell carcinoma. Clin Cancer Res. 2003;9(9):3406–12.
65. Shang ZJ, Liu K, Shao Z. Expression of chemokine receptor CCR7 is associated with cervical lymph node metastasis of oral squamous cell carcinoma. Oral Oncol. 2009;45(6):480–5.

Publisher's note